Boundary-Layer Meteorology
https://doi.org/10.1007/s10546-022-00705-w

RESEARCH ARTICLE

Wavelet Analysis of Coherent Structures Above Maize and Soybean Crops

Curto Lucia[1,2] · **María I. Gassmann**[1,2]

Received: 28 June 2021 / Accepted: 28 March 2022

Abstract
Turbulent coherent structures developed in the atmospheric surface layer are responsible for a large part of momentum and scalar fluxes exchanged with canopy layers. Their participation in processes such as evapotranspiration, pathogen infections, mechanical damage due to wind gustiness, modifies crop yield, with generally negative effects. Although South America has a variety of land covers, studies of these subjects are not common in the region. Here, we characterize the time scales of turbulent coherent structures above extensive maize and soybean crops using the wavelet methodology. The role of canopy-height changes associated with crop growth on turbulent structures development is analyzed. The effect of atmospheric stability on the characteristics of the structures detected is also studied. Wavelet analysis shows that both momentum and sensible heat are transported mostly by eddies of 350–400 s periods and also by more intense eddies of 40–50 s period. For momentum fluxes, the former period range prevails under strongly unstable conditions, while the second is present mostly under near-neutral situations. On the contrary, 40–50 s-lasting structures dominate the sensible heat transport under free convection conditions, while longer-lasting eddies transport heat in near-neutral conditions. Stability is the main factor allowing the coherent-structure topological classification, while the crop height is not important. Structures are identified through measurements performed at relative heights greater than those usually discussed in the literature, which indicates the need for further research into coherent-structure modelling.

Keywords Atmospheric boundary layer · Momentum transport · Roughness sublayer · Sensible heat transport · Surface layer

1 Introduction

Atmospheric turbulence generated in the atmospheric surface layer is driven by interactions between the airflow and the surface and modulated by the surface roughness and atmospheric

✉ Curto Lucia
lcurto@at.fcen.uba.ar

1 Departamento de Ciencias de la Atmósfera y los Océanos, Facultad de Ciencias Exactas y Naturales, Universidad de Buenos Aires, Av. Intendente Güiraldes 2160, Piso 1, Edificio Cero + Infinito, Cdad. Universitaria, C1428EHA Buenos Aires, Argentina

2 Consejo Nacional de Investigaciones Científicas y Técnicas (CONICET), Av. Godoy Cruz 2290, C1425FQB Buenos Aires, Argentina

stability conditions. Time series of micrometeorological measurements contain information about processes with different time and spatial scales. High-frequency velocity-component and atmospheric-scalar measurements show irregular time series. However, statistical techniques allow the identification of a level of organization throughout turbulent motion, known as coherent structures. Coherent structures provide an important contribution to momentum and scalar turbulent fluxes in the atmospheric surface layer (Katul et al. 1997; Thomas and Foken 2007). Some authors agree in identifying coherent structures as three-dimensional vortices or eddies, with some degree of coherence or organization of their motions in time and space (Theodorsen 1952; Adrian 2007; Wallace 2016). Coherent structures were first visualized under laboratory conditions in the 1960s (Kline et al. 1967). But realistic conditions under uncontrolled flow in the atmospheric boundary layer (ABL) make coherent structures identification more complex. Coherent structures present a characteristic vertical motion-pattern of updrafts (or ejections) followed by downdrafts (or sweeps) (Gao et al. 1989). Quadrant analysis is a technique for identifying the contribution of sweeps and ejections to mean turbulent fluxes of momentum and scalars (Shaw et al. 1983; Katul et al. 1997), as well as their contribution in time.

Wavelet analysis provides a suitable technique to detect coherent structures. Similarly to the Fourier transform, the wavelet transform allows rebuilding the original signal through the linear combination of variations of a mother function. In the Fourier transform, mother functions are sines and cosines, while the most common functions for the wavelet transform are the "Mexican hat", "Morlet" or "Haar" wavelets (Collineau and Brunet 1993). Wavelet transform has an important property, i.e., time-frequency location, which makes it capable of analyzing time series locally with the ability to "zoom in" and "zoom out" to small and large time scales, respectively. Analyzing time series of high-frequency atmospheric variable observations through wavelet variance allows the separation of structures with different time scales at different instants (Gao and Li 1993). Unlike the Fourier transform, it performs well on non-stationary signals. A remarkable skill of this tool is that the mean duration of periodic isolated events can be obtained through wavelet variance (Collineau and Brunet 1993).

The topology of coherent structures varies according to the scale and environment (Venditti et al. 2013) in the ABL. One of the main factors that influence topology is atmospheric stability (Dupont and Patton 2012). Thermal plumes are more likely to develop under unstable situations, while structures such as hairpin vortices are present in near-neutral conditions (Li and Bou-Zeid 2011). Structures associated with near-neutral regimes respond to relatively large scales, while smaller-scale coherent structures dominate under unstable situations. In intermediate situations, the two regimes coexist and both, large- and small-scale coherent structures are present (Smedman et al. 2007).

Several authors have studied coherent structures through wavelet analysis: Gao and Li (1993), Scarabino (2005) and Horiguchi et al. (2014), among others. Most of them based their analyses on momentum and scalar fluxes separately. However, there are few studies with turbulent variables measured above vegetated surfaces and even less those associated with annual crops developed in productive conditions and considering almost the entire growing season (Collineau and Brunet 1993; Brunet and Collineau 1994). Therefore, the aim of this work is to analyze the characteristic time scale of the coherent structures developed on cultivated surfaces under productive conditions and with growing plants (increasing height) applying wavelet analysis. Also, the effects of different stability conditions are studied.

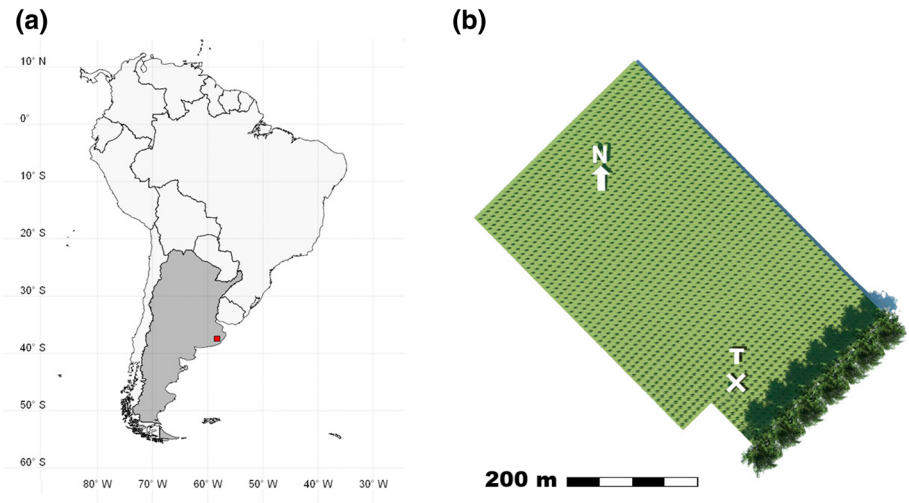

Fig. 1 Location of Balcarce (Argentina) (**a**), experimental site scheme showing the plot size and orientation, and instrument location (**b**)

2 Methodology

2.1 Experimental Set-up and Data Processing

Micrometeorological measurements above two crops—maize and soybean—are considered herein. Both experiments were performed in a 19-ha plot during the Southern Hemisphere summer growing season. The measurement site was located in an experimental farm owned by the School of Agricultural Sciences, National University of Mar del Plata and the Agriculture Experimental Site of the National Institute of Agricultural Technology (Instituto Nacional de Tecnología Agropecuaria-INTA) in Balcarce, Buenos Aires province, Argentina (Fig. 1a). The tower where instruments were located was installed inside the crop-plot (T in Fig. 1b). Meteorological and micrometeorological measurements were performed above an intermediate cycle maize (*Zea mays*) hybrid in the summer season 2011/2012, while measurements over an indeterminate soybean (*Glycine max*) hybrid were made in the summer 2012/2013. Because of the relative location of the experimental site with respect to the tower, only mean wind directions from the north-west to north-east sector were considered to have the flux footprint within the crop field. Both experiments were carried out in consecutive years during the austral summer, and were climatically similar, with a neutral phase of the El Niño Southern Oscillation. No significant regional temperature and air humidity anomalies were observed in both years. Precipitation had negative anomalies during January and February in both years, delaying maize and soybean growth and bloom.

Velocity components (u, v, w) and the sonic temperature (T) were measured at 20 Hz with a sonic anemometer (RM Young 8100, RM Young, Traverse City, Michigan 49686 USA). The sonic anemometer was placed at 5 m above ground level. Observations were made from 23 November 2011 to 29 February 2012 for maize; and from 3 January to 8 April 2013 for soybean. Profiles of air temperature, air humidity, and wind speed were measured at 15-min intervals in both experiments. Different vertical levels were considered for maize—2.40,

3.25, 4.40, 5.90, and 8.00 m—and for soybean—1.50, 2.10, 2.75, 3.70, and 6.05 m. Crop height (h) was monitored weekly for both crops.

Time series of micrometeorological variables were separated in 30-min intervals (called rounds), assuming the validity of Taylor's frozen turbulence hypothesis (Stull 1988). The coordinate system was aligned to the mean wind direction ($\overline{u}$) (Katul et al. 1997), with zero contribution in the cross-wind direction ($\overline{v}$). In the vertical direction, subsidence was negligible (Stull 1988), and it was verified that the mean vertical velocity component ($\overline{w}$) was zero. The analysis only includes periods during daytime. Reynolds decomposition was applied both for wind speed and air temperature, after which 30-min averages ($\overline{u}$, $\overline{w}$, and $\overline{T}$), perturbed values (u', w', and T') and covariances ($\overline{u'w'}$ and $\overline{w'T'}$) were calculated. These covariances are related to the turbulent vertical transport of momentum and sensible heat, e.g., see Stull (1988).

2.2 Surface-Layer Stability and Crop Height

In order to consider only well-developed turbulence rounds, thresholds were defined for each momentum and sensible heat flux:

$$\overline{u'w'} \leq -0.01 \text{ m}^2 \text{ s}^{-2}$$
$$\overline{w'T'} \geq 0.01 \text{ K m s}^{-1}$$

Periods were classified by stability conditions, considering the Obukhov length (L) (Foken 2017). As usual, L is negative during daytime; in atmospheric unstable situations, the non-dimensional stability parameter $z/L \leq 0$. Strongly unstable situations are defined accordingly Stull (1988), i.e., when $-1 \leq z/L \leq -0.5$. Free convection situations are considered when $z/L \leq -1$. In neutral conditions $L \to \infty$ (Stull 1988), and thus $|z/L| < 0.05$ is considered the cut-off value between neutral and unstable conditions. Summarizing, the ranges of the stability parameter that define each regime are detailed below:

Near-neutral (neutral and weakly unstable): $-0.05 < z/L \leq 0$
Unstable: $-0.5 < z/L \leq -0.05$
Strongly unstable: $-1 < z/L \leq -0.5$
Free convection: $z/L \leq -1$

Different crop height were classified according to ranges of z/h. For maize ($z/h < 3$, $3 < z/h < 5$, $z/h > 5$) were chosen differently than soybean ($z/h < 10$, $10 < z/h < 30$, $z/h > 30$), because the height vary along the vegetative phenological stages until the crops achieved their final heights. Maximum heights of maize and soybean were 0.75 and 1.80 m, respectively.

2.3 Quadrant Analysis

Quadrant analysis was performed on each round to quantify the contribution of sweeps and ejections to vertical turbulent transport of momentum ($u'w'$) and sensible heat ($w'T'$) (Wallace 2016). The covariability of the vertical velocity component and other atmospheric variables (here generalized as c'), makes it possible to define four quadrants (Q_i, i = 1 to 4) in the plane defined by c' and w' (Fig. 2), according to their sign (Table 1).

The flux contribution of each quadrant is defined as

$$S_i = \frac{\langle c'w' \rangle_i}{\overline{c'w'}}, \tag{1}$$

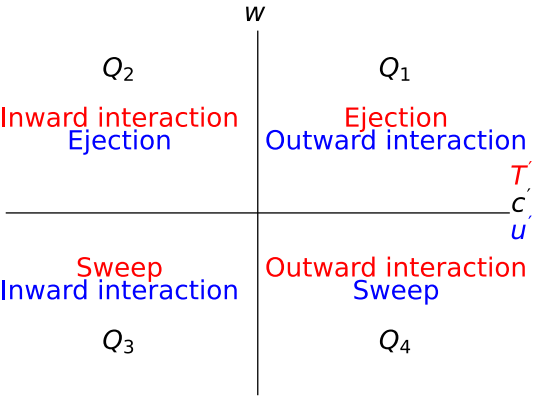

Fig. 2 Fluctuations of scalars and vertical wind velocity (c' and w') organized by sign in the four domain quadrants (Q_1, Q_2, Q_3, Q_4). Denomination of motion (ejection, sweep, inward or outward motion) for momentum ($c' = u'$, blue) and sensible heat transport ($c' = T'$, red)

Table 1 Quadrant number (Q_i, i = 1,2,3,4) according to the signs of c' and w'

Quadrant Q_i	Sign of c'	Sign of w'
Q_1	$c' > 0$	$w' > 0$
Q_2	$c' < 0$	$w' > 0$
Q_3	$c' < 0$	$w' < 0$
Q_4	$c' > 0$	$w' < 0$

where $\langle c'w' \rangle_i$ is obtained as the conditional average defined by

$$\langle c'w' \rangle_i = \frac{1}{N} \sum_{j=1}^{N} c'w'_j I_{i,j}, \tag{2}$$

$$I_i = \begin{cases} 1 & \text{if the point } (c', w') \text{ lies in } Q_i \\ 0 & \text{otherwise.} \end{cases} \tag{3}$$

Since the contributions are normalized, the sum of all S_i must be 1. Besides, $|S_i|$ must be less than or equal to 1 in order to identify dominant sweep and ejection processes, according to Nagano and Tagawa (1988) and Wallace (2016).

The time fraction of S_i in the 30-min period is denoted with τ_i, and expressed by

$$\tau_i = \frac{1}{N} \sum_{j=1}^{N} I_{i,j}, \tag{4}$$

where c' is u' for the momentum flux $u'w'$, and T' for sensible heat flux $w'T'$. In the surface layer, it is expected that $\overline{u'w'} < 0$ (Stull 1988). The major contributions to Reynolds shear stresses are S_2 and S_4, which are gradient-type motions corresponding to Q_2 and Q_4. For the sensible heat flux, $\overline{w'T'} > 0$ during daytime (Stull 1988), so the main contributions are from S_1 and S_3. Events in quadrants Q_4 and Q_2 define sweeps and ejections of momentum flux, respectively, and events in quadrants Q_3 and Q_1 define sweeps and ejections, respectively of scalar fluxes such as T' (Table 1 and Fig. 2).

2.4 Wavelet Analysis

To apply the wavelet method, every period of time series of u, w and T was transformed from 20 Hz into 1-s average time series. Wavelet transform (WT) is a local transform, which performs a time-frequency signal representation using any wavelet functions (Collineau and Brunet 1993). Wavelet functions divide a continuous-time signal into different scale components, assigning each a frequency range. This feature makes wavelets suitable for the study of non-stationary intermittent signals (Gao and Li 1993) like coherent structures. The wavelet transform of a time function ($f(t)$) is defined by

$$(WT_\psi f)(a,b) = \int_{-\infty}^{\infty} f(t)\frac{1}{a}\psi\left(\frac{t-b}{a}\right)dt, \tag{5}$$

where $\psi((t-b)/a)$ is the mother wavelet (previously called the mother function). The parameter a is associated with dilatation/narrowing of the wavelet function. It covers different frequency ranges, and preserves the area of the function—unlike the Fourier transform. Parameter b represents the displacement of the wavelet function in the time domain (Gao and Li 1993). Motions associated with coherent structures in the surface layer, such as sweeps and ejections, are intermittent and successive but non-stationary processes. As the width of $\psi((t-b)/a)$ can vary with changes in frequency, the wavelet transform has the ability to "zoom in" and "zoom out" to detect coherent structures of different time scales at different times (Gao and Li 1993). The "Mexican hat" (Eq. 6) wavelet function is used to detect the characteristic coherent structures time scale in the atmospheric turbulent flow of the surface layer, since it emerges as a second-order derivative of the Gaussian function (Gao and Li 1993; Chen and Hu 2003; Barthlott et al. 2007; Horiguchi et al. 2014),

$$\psi(t') = \left(1-t'^2\right)e^{-t'^2/2} \tag{6}$$

$$\int_{-\infty}^{+\infty} \psi(t')\,dt' = 0, \tag{7}$$

where $t' = (t-b)/a$. Equation 7 ensures the integration area remains constant as a and b change.

The wavelet variance (WV) can be interpreted as proportional to the signal energy. The local maximum is used to identify the time scale of main turbulent eddies transporting momentum or scalars in the atmospheric surface layer (Collineau and Brunet 1993). The wavelet variance is obtained from the discrete expression given by Dale and Mah (1998)

$$WV(a) = \sum_{k=1}^{N} (TW_\psi f)^2(a,b_k)/N, \tag{8}$$

where k is a counter, and N is the maximum amount of data in that interval (1800, 30-min data at 1 Hz). Local peaks of WV and their corresponding time scales were identified for u' and w' for momentum transport. The same methodology was applied for w' and T' for sensible heat transport. The four most energetic local peaks in each period were considered. No peaks were detected in some of the periods, which were discarded from the analysis.

3 Results and Discussion

The number of 30-min periods of fast-response measurements of u, w and T registered during the sampling period amount to 3644 and 4209 for maize and soybean, respectively.

Table 2 Classification of 30-min periods by atmospheric stability

Crop	Stability condition	Total cases	Flux		
			$\overline{u'w'}$	$\overline{w'T'}$	Both
Maize	Near-neutral	33	16	2	15
	Unstable	126	6	66	54
	Strongly unstable	54	0	52	2
	Free convection	142	0	142	0
Soybean	Near-neutral	266	62	16	188
	Unstable	179	16	27	136
	Strongly unstable	34	0	28	6
	Free convection	43	0	43	0

From those rounds, 722 —19%—for maize and 1029—24%—for soybean correspond to the mean wind from the north-west–north-east sector. After applying the criteria defined in Sect. 2.2, 336 rounds transporting sensible heat are selected over the maize canopy (47% of total rounds considered), and 444 (43%) over soybean. The evaluation for the momentum flux yields 112 (16%) cases in maize and 674 (66%) cases in soybean. The difference in number between sensible heat and momentum rounds is minor in the soybean crop, but in maize, the number of cases with thermal-driven turbulence—i.e. high $\overline{w'T'}$ and low $|\overline{u'w'}|$ values—is greater than shear-driven turbulence—i.e. high $|\overline{u'w'}|$ and low $\overline{w'T'}$ values.

Identified periods are classified by stability conditions according to the Obukhov length. The number of cases obtained for each flux and crop type is shown in Table 2. Free convection, strongly unstable and unstable cases outnumber near-neutral cases in maize, but the opposite is observed in soybean. At the maize plot, turbulence transports both momentum and sensible heat (around 50% cases) well in near-neutral conditions, or even only momentum (the other half of cases), since in those cases the value of $\overline{w'T'}$ is negligible (Table 2). A significant number of sensible-heat-flux periods occur in unstable and especially in strongly unstable and free convection conditions in maize. From these cases, 52% is associated with sensible heat flux only, while in the remainder, turbulence is transporting fluxes of momentum and sensible heat together in unstable situations. Turbulent structures develop in strongly unstable and free convection conditions transport effectively exclusively sensible heat (194 cases), while in only two detections both momentum and sensible heat are transported. Most of the selected cases in soybean are observed in near-neutral conditions, and 188 of 266 rounds correspond to turbulence transporting both momentum and sensible heat. Under unstable conditions, 76% of cases transport both fluxes altogether, while the rest transport only sensible heat or momentum (Table 2). The sensible heat flux prevails in both maize and soybean under strongly unstable conditions, with only a few cases of both, and no cases associated with momentum flux. For free convection situations, there are only cases associated with the sensible heat flux.

These results clearly indicate that in near-neutral situations both sensible heat and momentum are transported jointly. This behaviour has also been observed by others (Li and Bou-Zeid 2011). Turbulent eddies acquire a hairpin-vortex topology, with a complex horizontal pattern of vortex interaction outlined by Finnigan (2000). Sensible heat transport prevails in strongly unstable and free convection conditions, as could be seen particularly in maize. Thermal plumes develop in free convective conditions (Stull 1988), which transport scalars (like T') more effectively (Li and Bou-Zeid 2011).

Table 3 Mean ratio of ejections versus sweeps for both momentum and sensible heat transport according to stability and relative measurement height for 30-min periods in maize and soybean crops

Flux Stability condition	Maize			Soybean		
	z/h					
	< 3	3–5	≤ 5	< 10	10–30	≤ 30
$u'w'$ S_2/S_4						
Near-neutral	0.52(20)*	0.69(11)*	–	0.96(187)	0.94(63)	–
Unstable	0.61(44)	0.61(14)	0.67(2)	1.01(125)	0.93(24)	0.87(3)
Strongly unstable	0.56(2)	–	–	0.99(5)	0.86(1)	–
Free convection	–	–	–	–	–	–
$w'T'$ S_1/S_3						
Near-neutral	0.88(9)	1.05(9)	–	1.15(150)	1.11(53)	1.21(1)
Unstable	1.15(58)	1.12(60)	1.23(2)	1.07(140)	1.31(20)	0.97(3)
Strongly unstable	1.29(35)	1.27(17)	1.16(2)	1.44(27)	1.56(6)	2.29(1)
Free convection	1.30(83)	1.31(59)	–	1.34(35)	1.49(8)	–

The number of cases averaged in each bin is depicted in parentheses. Significance of differences (p value $<$ 0.05) between mean values for each crop and each stability is indicated (*)

Quadrant analysis of selected periods reveals that sweeps prevail in intensity over ejections for momentum transport in both crops, as S_2/S_4 values are less than 1 (Table 3), except for unstable cases in soybean with z/h less than 10. For each stability regime and for each crop type, the S_2/S_4 mean values according to the z/h ranges reveal almost no significant differences, except in maize for near-neutral cases. For sensible heat fluxes, ejections are stronger than sweeps ($S_1/S_3 > 1$) in both crops (Table 3). Exceptions are found for maize with $z/h < 3$ under near-neutral conditions and soybean with $z/h \leq 30$ in unstable situations (with only three cases). However mean values of S_1/S_3 obtain for the analyzed z/h ranges do not differ significantly for each stability regime and crop. Because of this analysis the development of turbulent structures does not show a dependency with crop height.

Turbulence reveals a different behaviour relative to atmospheric stability and crops. In the case of maize, as instability increases, the ratio S_2/S_4 decreases weakly from 0.60 in near-neutral to 0.56 in strongly unstable situations, indicating that ejections become slightly less dominant over sweeps in unstable and strongly unstable regimes (Table 4). However, no significant differences between these values are found. For soybean, the opposite variation is observed: the ratio is higher as instability increases. The S_2/S_4 values change from 0.93 in near-neutral and 0.95 in unstable to 1.00 in strongly unstable, with statistically significant differences (Table 4). Other authors, e.g. Shaw et al. (1983), have shown that sweeps for $u'w'$ are usually more intense. The study of the duration of each quadrant event (Eq. 4) shows that sweeps are present longer than ejections ($\tau_2/\tau_4 < 1$) over maize in unstable and strongly unstable regimes, while the opposite is found for in the soybean crop ($\tau_2/\tau_4 > 1$). Despite these findings, the rate τ_2/τ_4 decreases with instability (Table 4). This result means that sweeps for momentum transport become stronger and last longer as instability increases in the maize experiment. In the soybean experiment, sweeps are the strongest vertical movement but they are weaker than in maize—and even equal to ejections in strongly unstable—and ejections last longer with less instability. There are no cases of $u'w'$ associated to free convection situations, indicating that in free convection conditions, developed turbulent structures do not transport net momentum.

Table 4 Mean ratio of ejections versus sweeps for both momentum and sensible heat transport and their mean duration, according to stability conditions, for 30-min periods in maize and soybean

Crop	Stability condition	$u'w'$		$w'T'$	
		S_2/S_4	τ_2/τ_4	S_1/S_3	τ_1/τ_3
Maize	Near-neutral	0.60(31)	1.00	0.88(17)*	0.96
	Unstable	0.62(60)	0.83	1.15(120)*	0.83
	Strongly unstable	0.56(2)	0.61	1.28(54)*	0.79
	Free convection	–	–	1.31(142)	0.79
Soybean	Near-neutral	0.93(250)	1.10	1.13(204)	1.49
	Unstable	0.95(152)	1.08	1.08(163)*	0.98
	Strongly unstable	1.00(6)*	1.03	1.49(34)*	0.89
	Free convection	–	–	1.37(43)	0.89

The number of cases averaged at each bin is depicted in parentheses. Significance of differences (p value $<$ 0.05) between mean values for each crop is indicated (*)

For sensible heat fluxes, ejections are stronger than sweeps in both crops, as mentioned before (Tables 3 and 4). The ratio S_1/S_3 is greater than 1 in all cases, except for near-neutral cases in maize. This ratio increases also with instability over both crops, with significant differences between near-neutral, unstable and strongly unstable (Table 4). Sweeps last longer than ejections ($\tau_1/\tau_3 < 1$) except under near-neutral in soybean (Table 4). However, τ_1/τ_3 decreases with increasing instability, revealing that sweeps are weaker than ejections, and yet contribute longer to sensible heat transport in strongly unstable and free convection situations. As was mentioned before, thermal plumes develop in free convective situations, with strong ejections over a confined area, surrounded by weak sweeps extending in space and longer-lasting (Stull 1988).

Wavelet analysis is applied to periods previously analyzed (Table 2) and classified according to the stability regimes defined in Sect. 2.2. Figure 3 shows the wavelet transform of u' ($WT(u')$), w' ($WT(w')$) and T' ($WT(T')$) for a selected round of the maize experiment, and their respective 30-min time series. The wavelet transform preserves the sign of the variable on which it is applied. For example, at the beginning of its time series, u' is mostly negative (Fig. 3b) and it has associated negative values of $WT(u')$ (blue values before 300 s in Fig. 3a). The same pattern appears between 700 and 900/1000 s, and from 1700 to 1800 s. On the contrary, in period intervals 400–600 s and 1000–1700 s, $u' > 0$ and $WT(u')$ is positive as well (red), as seen in Fig. 3a. Then, u' become slightly negative—between 700 and 900/1000 s—with corresponding negative values of $WT(u')$ (blue in Fig. 3a) in 700–900 s. From 1200 to 1700 s, u' is again mainly positive, and at the end of the time series it turns negative again (Fig. 3b). The wavelet transform of u' shows the same behaviour, with positive (red) values up to 1700 s, and then negative (blue) until the end of the time series (Fig. 3a). Similar behaviour (in terms of sign) is detected for the w' (Fig. 3d) and T' (Fig. 3f) time series and their respective wavelet transforms $WT(w')$ (Fig. 3c) and $WT(T')$ (Fig. 3e).

Figure 3 shows that positive (negative) values of $WT(w')$ (Fig. 3c) correspond to positive (negative) values of $WT(T')$ (Fig. 3e), and with negative (positive) $WT(u')$ (Fig. 3a), in concordance with the signs of momentum and sensible heat flux. The negative value of $\overline{u'w'}$ indicates that near-surface atmospheric turbulence transports momentum downwards to the surface to compensate for its loss due to drag forces. As $\overline{u'w'}$ is a 30-min average of what eddies are transporting, the detailed wavelet analysis along the period shows that turbulence

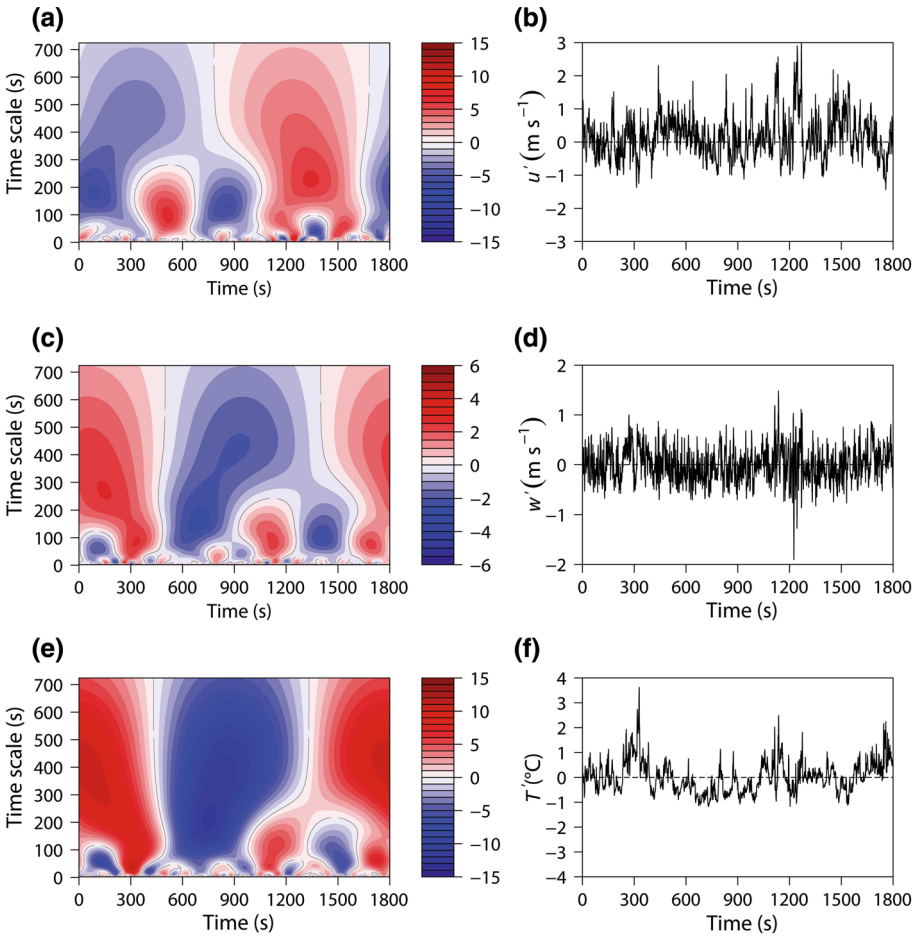

Fig. 3 Wavelet transform of perturbed horizontal [(**a**), $WT(u')$] and vertical [(**c**), $WT(w')$] wind components, and temperature [(**e**), $WT(T')$], and their respective 1-s time series [(**b**, **d**, **f**)]. The 30-min period corresponds to 1300–1330 LT (local time = UTC − 3 h), 17 December 2011, in the maize experiment, with $z/L = -1.20$ (free convection)

transports momentum downwards in some moments and upwards in others. What the quadrant analysis shows is that in the 30-min period weak sweeps transport more momentum downward than that transported upward by intense ejections. The positive value of $\overline{w'T'}$ indicates sensible heat is transported by eddies from the surface to the atmosphere, because during daytime the land surface is warmer than the air, and acts as a heat source in unstable conditions (if advection processes are neglected). Alternation between positive and negative WT along the analyzed period (Fig. 3a, c, e) shows the characteristic behaviour of coherent structures (Gao and Li 1993). This behaviour is also visible at different time scales: alternation of positive and negative values of high-frequency events and structures of larger scale (extreme values corresponding to 50 and 450 s, respectively). The particular case presented in Fig. 3 corresponds to a free convection situation. In this period, there are found contributions of time scales with two maximum in 50 s and 400 s for both w' (Fig. 3c) and T' (Fig. 3d), consistent with a significant $w'T'$ transport. For u', maximum wavelet variance corresponds

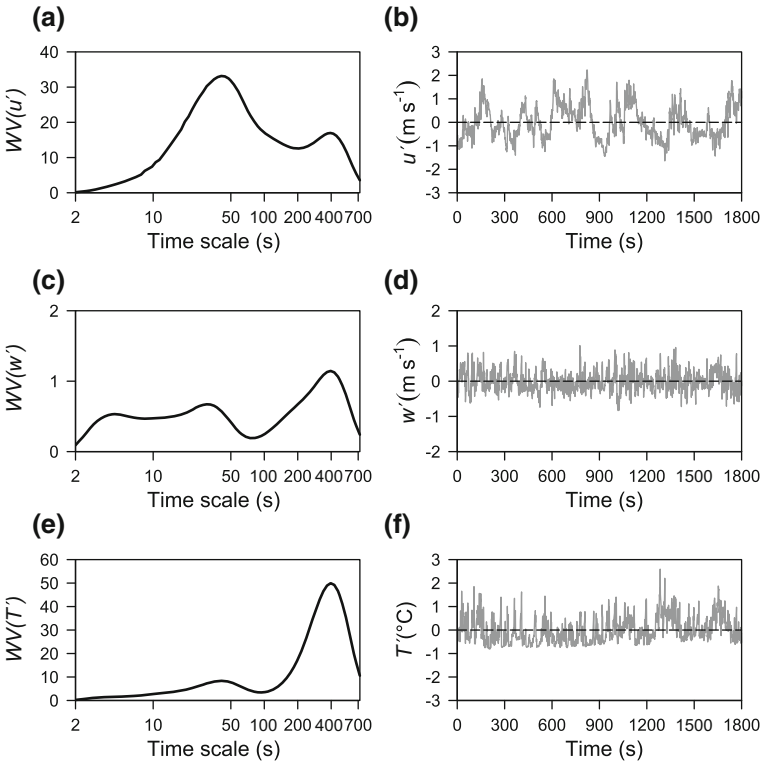

Fig. 4 Wavelet variance of perturbed horizontal [(**a**), $WV(u')$) and vertical ((**c**), $WV(w')$] wind components, and temperature [(**e**), $WV(T')$], and their respective time series [(**b**, **d**, **f**). The 30-min period corresponds to 1600–1630 LT (local time = UTC − 3 h), 3 February 2013, in the soybean crop, with z/L = –0.68 (strongly unstable)

to time scales near 200 s (Fig. 3a), not matching time scales of w'. This feature explains the negligible momentum flux observed for free convection stability conditions.

The characteristic time scales of the coherent structures is determined through the wavelet variance calculated with the wavelet analysis. Figure 4 shows an example of wavelet variance for the three turbulent variables of a round selected from unstable cases during the soybean growing season. The shape of the wavelet variance with its local maximum shows the time scale of coherent structures processes and their contribution to vertical transport. Beginning with the analysis of w' (Fig. 4c), there is random background turbulence at scales less than 10 s, high-frequency events between 10 s to 40–50 s (∼1 min), and large-scale structures of 400–450 s (6–7 min). The distribution of energy explained by the wavelet variance of u' (Fig. 4a) and T' (Fig. 4e) also reveals turbulent events corresponding to scales of 40–50 s and 400–450 s. According to Gao and Li (1993), turbulence with a time scale of 6–7 min corresponds to ABL structures, while high-frequency events with scales near 50 s are associated with small-scale turbulence in the surface layer.

The time series of u' (Fig. 4b) shows a high variability depicted by rapid and intense changes. The alternation of sweeps and ejections—a signature of coherent structures—produces rapid changes in turbulent variables, visualized as ramps in the time series (Shaw et al. 1989). In Fig. 4b, those quick and intense changes in u' (ramps) indicate the presence

of coherent structures with 1-min frequency or less. In $WV(u')$, the most intense local peak corresponds to the time scale of 40–50 s (Fig. 4a), in agreement with the high-frequency events mentioned before. At the same time, Fig. 4b shows longer-lasting ramps: from 100 s to 400 s, from 600 s to 900 s, from 1000 s to 1400 s, and from 1400 to 1700 s. In all cases, there is a decline in u' values (from positive to negative), followed by a sharp increase (from negative to positive) that last $\approx$ 300–400 s. The second peak in $WV(u')$ (Fig. 4a) corresponds to those ramps, with a characteristic time scale near 400 s.

The round analyzed in Fig. 4 shows that $WV(w')$ (Fig. 4c) also has characteristic time scales of 400 s, 40–50 s, and less than 10 s, according to the importance of the variance explained by each time scale. The relative difference between the energy explained by each local peak is less than that seen in $WV(u')$ (Fig. 4a). The corresponding w' time series (Fig. 4d) illustrates the characteristic variability of atmospheric turbulence, with overlapping ABL structures and high-frequency events. The wavelet variance of T' (Fig. 4e) shows two local peaks, related to characteristic time scales of near 400 s and 40 s—in that order of importance. The corresponding time series (T', Fig. 4f) shows high-frequency variability (less than 1 min), but also ramps of greater duration. From the beginning and up to 300 s, T' decreases from positive to negative values, increases from 800 s to 1100 s, drops again from 1300 to 1700 s, and finally increases from 1600 to the end. While both 40 s and 400 s represent the characteristic time scales of coherent structures' in this round, it can be easily concluded that the high-frequency or small-scale eddies are responsible for the $u'w'$ transport above both canopies, while those ABL-scale eddies are responsible for transporting energy in the form of sensible heat (average of $w'T'$).

As an example of the information provided by wavelet variance about the time scale of dominant processes, we present the analysis of a second case of coherent structures for a round of the soybean experiment (Fig. 5). The three variables (u', w', T') reveal structures with maximum variance in the time scale of 400 s or 6–7 min (Fig. 5a, c, e). On the other hand, the time series of the three variables show ramps starting at around 1200 s and ending at 1600 s (dashed lines in Fig. 5b, d, f), which are associated with the presence of coherent structures in the field. As u' increases, w' decreases, and the same occurs with T', in accordance with the signs of the fluxes ($\overline{u'w'} < 0$ and $\overline{w'T'} > 0$). A second process is seen in the sensible heat flux at 100 s (Fig. 5c, e) which has, in both w' and T' time series, ramps of the same duration (dot–dashed lines in Fig. 5d, f). In this case, the wavelet variance analysis and the time series pattern reveal that there are coherent structures transporting both momentum and sensible heat or only sensible heat depending on the time scale of the eddies involved.

The characteristic coherent-structure time scale of $WV(u')$ corresponds to 400–450 s. In the same round, $WV(w')$ also shows a local maximum near 400 s (Fig. 5c). Therefore, the coherent structures associated with momentum flux of that particular round has a characteristic time scale of 6–7 min. Ramps with the same period can be seen in the u' time series: increasing u' values between 1200 and 1500 s, and then decreasing between 1500 and 1700 s. At that same time, an opposite behaviour is seen in w': decreasing between 1200 and 1500 s, and increasing between 1500 and 1750 s (dash-dotted lines in Fig. 5d). As a result of this interaction, the instantaneous value $u'w'$ is < 0 according to the sign of momentum flux. Those ramps last approximately 350–400 s, in concordance with the characteristic time scale of u' and w' found through the wavelet variance.

The wavelet variance of w' reveals another maximum at approximately 100 s, besides the most energetic one at 400 s ($WV(w')$, Fig. 5c). The maximum wavelet variance of T' ($WV(T')$, Fig. 5e) has the same characteristic time scale as w'. In this round, the time scales of the coherent structures transporting sensible heat are 100 s and 400 s. In the w' and T' time series (Fig. 5d, f) ramps can be seen that last approximately 100 s (dash–dotted lines

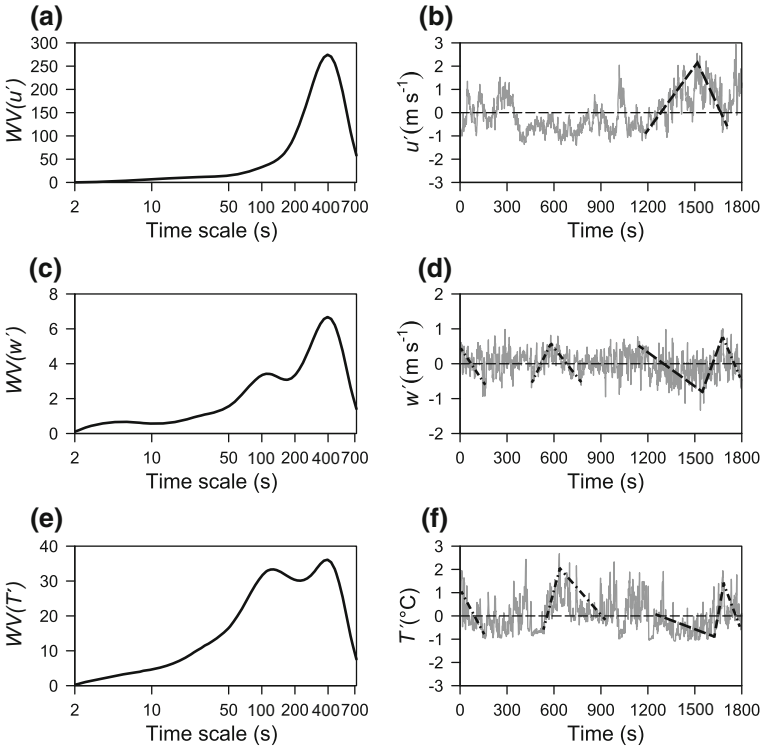

Fig. 5 Wavelet variance of perturbed horizontal [(**a**), $WV(u')$] and vertical [(**c**), $WV(w')$] wind components, and temperature [(**e**), $WV(T')$], and their respective time series [(**b**, **d**, **f**)] The 30-min period corresponds to 1330–1400 LT (local time = UTC − 3 h), 3 March 2013, in soybean crop, with z/L = –0.51 (strongly unstable)

in Fig. 5d, f), and 350–400 s (dashed lines in Fig. 5d, f). Besides, w' and T' ramps have the same behavior at the same time: when w' increases in values, so does T', and when w' decreases, T' does as well. As this round corresponds to daytime (1330–1400 h) and unstable conditions (z/L = -0.51), coherent structures are consistent with $w'T' > 0$.

The distribution of characteristic time scales (according to local peaks in wavelet variance) for all rounds with coherent structures presence is presented in Fig. 6. In free convection cases (Fig. 6a, c) the most prevailing eddies are those with characteristic time scales between 350 and 400 s, for T', with relative frequencies of 0.4 in maize (Fig. 6a) and 0.5 in soybean (Fig. 6c). Next in importance (in terms of energy), are eddies with time scales up to 50 s (small-scale eddies, period less than 1 min), with relative frequencies of 0.2, for both maize and soybean. Between 50 and 350 s, the relative frequency of eddies decreases to approximately 250 s. There are almost no differences in frequencies between T' and u' in near-neutral cases for both crops (Fig. 6b, d). However, there are no cases of u' in free convection cases (Fig. 6a, c), due to no $u'w'$ transport under that stability regime—only $w'T'$. For w', small-scale eddies dominate in importance (characteristic time scales up to 50 s), with relative frequencies of 0.5 for maize (Fig. 6a) and 0.4 for soybean (Fig. 6c). The next most frequent time scales are between 350 and 400 s, with relative frequencies of 0.3 for both crops. There are few cases with time scales between 200 and 250 s, with relative frequencies less than 0.2. From the analysis of all rounds with strong unstable conditions, almost no cases of coherent structures'

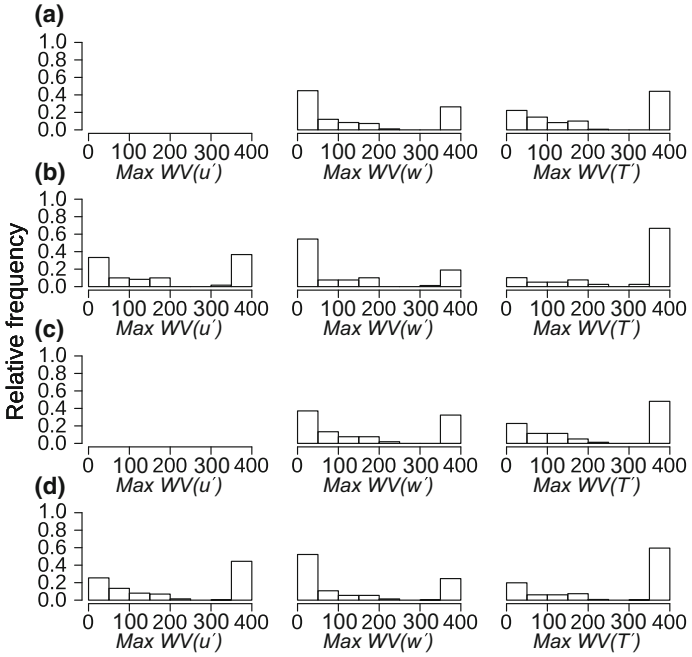

Fig. 6 Histogram of relative frequencies of maximum wavelet variance of u', w' and T', over maize (**a**, **b**) soybean (**c**, **d**) 30-min rounds under free convection (**a**, **c**) and near-neutral conditions (**b**, **d**)

time scales between 250 and 350 s are observed in the three variables, in agreement with the specific cases shown in Figs. 4 and 5. Also, there are no contributions from values greater than those presented in Fig. 6, even though time scales of up to 725 s are considered. There are no significant differences with unstable and strongly unstable regimes (not shown).

In near-neutral conditions the relative frequency of scales up to 50 s is greater than in free convection cases for w' in both crops and for scales between 350–400 s for T' (Fig. 6b, d). Also, in near-neutral the contributions of scales between 350–400 s is greater for u', and scales up to 50 s contribute more in maize cases (Fig. 6b). The frequency of occurrence of scales between 50 and 350 s is negligible in both crops. This feature is clearer in near-neutral cases (Fig. 6b, d). Also, there is a more organized frequency decay as time scale increases (from 0–50 to 300–350 s) under the free convection regime (Fig. 6a, c).

Over maize, the relative frequency of time scales up to 50 s is 0.35 in near-neutral cases ($Max\ VW(u')$ in Fig. 6b), while there are no cases in free convection ($MaxVW(u')$ in Fig. 6a). For soybean the same behaviour is observed in free convection, and the relative frequency of time scales up to 50 s is a little smaller in near-neutral cases (0.3) ($Max\ VW(u')$ in Fig. 6d). The frequency of coherent structures with larger time scales (350–400 s) above maize is almost the same as smaller scales (0.4) ($Max\ VW(u')$ in Fig. 6b). Over soybean that difference is greater, with a relative frequency of 0.5 for greater scales ($Max\ VW(u')$ in Fig. 6d). Turbulence with time scales between 50 and 350 s has less contribution. The behaviour for u' in unstable and strongly unstable cases is similar to near-neutral (see supplementary information).

The same analysis applied to w' shows that relative contributions of time scales up to 50 s are less in free convection than near-neutral conditions, in maize ($Max\ VW(w')$ in Fig. 6a,

Table 5 Horizontal spatial and time scales of coherent structures, and maximum mean wind speed ($\overline{u}$), by crop type and atmospheric stability status

Crop	Atmospheric stability	Max $\overline{u}$ (m s^{-1})	Time scale (s)	Horizontal scale (m)
Maize	Near-neutral	6.3	400	2512
			48	301
	Free convection	1.4	400	576
			44	63
Soybean	Near-neutral	11.7	400	4664
			41	478
	Free convection	1.3	400	532
			41	55

b) and soybean cases ($Max\ VW(w')$ in Fig. 6c, d). Overall, in maize cases the contribution from intermediate time scales is small under near-neutral as well as under free convection situations ($Max\ VW(w')$ in Fig. 6a, b). At the same time, the relative frequency of less-contributing time scales remains the same in both stability situations over soybean. There are also almost zero contributions between 250–350 s, as mentioned before.

The behaviour between near-neutral and free convection cases of T' is different from that w'. In free convection situations over maize, the relative frequency of processes with 350–400 s time scales is 0.45, while in near-neutral conditions it is 0.7 ($Max\ VW(T')$ in Fig. 6a, b). In soybean, relative contributions are 0.5 and 0.6, for free convection and near-neutral, respectively ($Max\ VW(T')$ in Fig. 6c, d). In near-neutral cases—where $\overline{w'T'}$ is smaller—the poor sensible heat transport that could take place in the roughness sublayer or the surface layer seems to be carried out by large-scale eddies, with characteristic time scales between 350 and 400 s. The relative contribution of time scales up to 50 s is more important in free convection than near-neutral cases: 0.25 and 0.15 in maize ($Max\ VW(T')$ in Fig. 6a, b), and 0.2 in soybean ($Max\ VW(T')$ in Fig. 6c, d). Near-neutral cases have almost no contribution from other time scales than 0–50 and 350–400 s (relative frequencies of greater than 0.6), and little contribution from scales of 50–200 s.

The (horizontal) spatial scale of eddies associated with coherent structures can be calculated using the mean wind speed ($\overline{u}$) (Gao and Li 1993). Mean wind speeds $\overline{u}$ are estimated as the average of the mean wind speeds of all rounds whose maximum WV corresponds to the associated time scale. The maximum $\overline{u}$ is then selected to find the maximum coherent structures' horizontal scale. Table 5 shows spatial scale estimations in free convection and near-neutral situations for both crops. For time scales up to 50 s (values between 40 and 50 s), the horizontal scale of those coherent structures is longer in near-neutral (up to 478 m) than free convection situations (55-63 m) over both crops because the $\overline{u}$ of the former is higher (Table 5). Coherent structures with time scales near 40–50 s above both crops have spatial scales of the order of 10^1m in agreement with the 83–112 m found by Gao and Li (1993). Unstable and strongly unstable situations reflect intermediate values between near-neutral and free convection (not shown).

For time scales of 400 s, the spatial scales of coherent structures range between 530 and 4600 m (Table 5). The larger scales correspond to coherent structures developed over soybean in near-neutral conditions, with mean wind speeds up to 11 m s^{-1}. The smallest scales correspond to free convective regimes, with weaker mean wind speed (1.4 and 1.3 m s^{-1}, over maize and soybean respectively). Coherent structures with time scales of 6–7 min

have horizontal scales of the order of 10^3 m—which are typical of ABL eddies (Stull 1988). High variability in the horizontal space-scale due to mean wind was also observed by Gao and Li (1993).

Differences in coherent structures scales (both in time and space) can be explained by changes in coherent structures' topology caused by changes in stability conditions. The influence of crop height increase in coherent structures behaviour is negligible in comparison to stability effects, as shown in Table 3. Hairpin vortices structures dominate in neutral and slightly unstable situations (Li and Bou-Zeid 2011) (near-neutral in our study). Structures of this type transport momentum and scalars altogether, in concordance with the results shown in Table 2 for both fluxes. Results show more situations associated with $u'w'$ transport exclusively or with both $u'w'$ and $w'T'$. In structures like hairpin vortices, measurements performed at relative heights (z/h) close to the canopy top, e.g., $2.8h$ over maize, reveal that sweeps dominate over ejections in strength but have the same duration as structures like hairpin vortices, in concordance with the results in Table 4. As the relative height above the canopy increases, the contribution of ejections to property transport is greater, but does not exceed the contribution of sweeps (Shaw et al. 1983). In the soybean experiment, where measurements were performed at $6.7h$, ejection equal sweep contributions to momentum turbulent transport. Also, ejections have a longer duration than sweeps under near-neutral stability conditions. The wind profile in the roughness sublayer (within the canopy mixing layer) reveals a weak mean wind speed inside the canopy (Finnigan 2000), and strong mean wind shear at the canopy top. The shear stress causes Kelvin–Helmholtz instability to develop, with the consequent generation of horizontal rollovers and the typical hairpin vortices. This type of coherent structures stretches in the horizontal plane, in the crosswise direction, reaching 4600 m (Table 5). Therefore, hairpin vortices would dominate turbulent fluxes above both crops in near-neutral regimes, with characteristic time scales between 350 and 400 s (6–7 min).

Thermal plumes develop under free convective situations, and turbulent transport of scalars dominates over momentum transport (Li et al. 2005). Table 2 shows a greater proportion of cases associated with sensible heat than momentum flux in strongly unstable situations, with no structure detection associated to momentum transport in free convection conditions. Thermal plumes develop with rapid intense ejections occupying a reduced area surrounded by extended and slow weak sweeps. Table 4 shows this behaviour for $w'T'$, with $S_1/S_3 > 1$ in almost all cases, and $\tau_1/\tau_3 < 1$. Weak mean wind speeds favour the development of this plume-type structure caused by thermal forcing. Thermal plumes are more extended in the vertical plane and not so much in the horizontal. Strongly unstable and free convection situations promote the turbulent scalar transport—as $w'T'$—and small-scale turbulence coherent structures whose characteristic time scale is between 40 and 50 s (less than 1 min).

According to Finnigan (2000) canopy-mixing layer characteristic prevail up to $3h$—three times the crop height. Micrometeorological measurements above maize correspond to a height of at least $2.8h$. In this layer, turbulent fluxes would enhance instability more intensely, and benefit scalar transport over momentum (Li and Bou-Zeid 2011). Sweeps transporting momentum are more intense close to the canopy top (analyzed over maize in this study) and last longer than ejections (Table 4). This phenomenon intensifies with increasing instability. For sensible heat, sweeps are weaker and last longer than ejections with increasing instability. Measurements above soybean correspond to $6.7h$ in the surface layer where near-neutral and neutral conditions prevail. Coherent structures would behave as hairpin vortices, with a complex horizontal pattern of sweeps and ejections capable of transporting scalars and momentum vertically altogether (Foken 2017). As the measurement height is moving farther from the canopy top, the relative contribution of ejections increase without becoming domi-

nant in strength but so in duration, with S_2/S_4 average values still lesser than 1 (as over maize) and $\tau_2/\tau_4 > 1$. Also the space scale of dominant structures increases, regardless of instability. Both types of coherent structures are observed in intermediate unstable conditions, with time scales gradually evolving from 40–50 s to 350–400 s.

4 Conclusions

The characteristics of turbulence coherent structures are studied in two experiments over a surface covered with maize and soybean measured during daytime hours. Micrometeorological measurements are analyzed through quadrant analysis to determine contributions of sweeps and ejections to momentum and sensible heat turbulent fluxes. The characteristic time scale of coherent structures is determined by means of wavelet analysis. Measurements above crop canopies were performed at different relative canopy heights. Two different crops are analyzed (maize and soybean) along their growing season. Over maize, fast-response sensors were installed in the roughness sublayer, while over soybean, they were installed in the surface layer (Finnigan 2000) where the Monin–Obukhov similarity theory is valid. Canopy mixing layer conditions prevail above maize, with more cases of strongly unstable and free convection environments where coherent structures develop as thermal plumes. On the other hand, coherent structures evolve above the soybean crop in the surface layer, with 50% of cases in near neutral or neutral stability conditions, where hairpin vortices prevail.

Two different types of turbulent transport (momentum and sensible heat) are analyzed altogether. There are more 30-min rounds with significant sensible heat—$w'T'$—transport than momentum —$u'w'$—transport in the maize experiment: 47 and 18%, respectively. On the contrary, more structures are identified transporting momentum (66%) than sensible heat (43%) in the soybean experiment.

Sweeps are more intense than ejections in momentum fluxes, and are present longer in time, especially above maize. In soybean, ejections last longer because of the greater distance to the canopy top. As pointed out in Shaw et al. (1983) sweeps explain the total amount of momentum flux better. For $w'T'$, ejections explain most of the sensible heat transported and thermal plumes are the best model to explain air motion. Intense ejections in a reduced area are an efficient structure for the transport of sensible heat. Weak and longer-lasting sweeps stretch over a greater area around ejections.

Wavelet variance makes it possible to identify characteristic coherent-structure time scales. Results of T' and u' in both crops shows that both momentum and sensible heat are transported predominantly by eddies of 350–400 s time scales, and in a second place by periods up to 50 s. Coherent structures with greater time scales correspond to ABL structures, while the smallest correspond to high-frequency (or small-scale) turbulence. This pattern is observed in both stability conditions (near-neutral and free convection conditions). However, energy processes are dominated mainly by small-scale eddies in w'.

Atmospheric stability regimes determine the behaviour of coherent structures: 350–400 s time scales prevail under free convection situations, in contrast to greater proportion of structures of up to 50 s transporting u' and w' in near-neutral rounds. However, the proportion of eddies of up to 50 s transporting T' is greater in free convection. Sensible heat transport is carried out by larger-scale eddies, because transport under near-neutral conditions is weak. Stability regimes affect the development of coherent structures by modifying their topology. Hairpin vortices prevail in neutral and weak unstable situations, associated with high-frequency structures. Thermal plumes gain relevance with increasing instability, and

ABL structures become dominant under strongly unstable regimes. Similar to the changes in coherent structures type with stability, turbulent momentum and sensible heat fluxes also show different behaviour. They are transported by structures whose characteristic time scale was between 350 and 400 s in near-neutral conditions. Under free convection situations, sensible heat transport prevails, associated with plume patterns, momentum is not transported by coherent structures. Thermal plumes' characteristic time scale is between 40 and 50 s (less than 1 min).

Measurements in the maize experiment were performed at a height of $2.8h$, within the canopy mixing layer, under strong instability conditions that promote the development of vigorous thermal plumes. In the soybean experiment, measurements were at a height of $6.7h$, in the surface layer, with less intense instability. The most intense mean wind over soybean enable the prevalence of hairpin vortices with horizontal scales of up to 4000 m. Both types of coherent structures are observed in intermediate stability conditions. There are few cases with time scales between 200 and 250 s, and no cases of coherent structures time scales between 250 and 350 or greater than 400 s (time scales up to 725 s are considered).

The kind of information about turbulence that can be obtained from quadrant and wavelet analysis is different and complementary. Quadrant analysis focuses on the coherence of Reynolds stresses through the contribution from the four quadrants defined by the signs of the two turbulent variables that determine turbulent transport ($u'w'$ in the case of momentum and $w'T'$ in the case of sensible heat). On the other hand, wavelet analysis focuses on the time scale of the processes involved in the time series under study. Therefore, a thorough analysis of turbulence characteristics above canopies would require using both methodologies to obtain robust results.

The field experiments were carried out in productive plots, with crop heights varying throughout the growing season. The stability condition is the main influence on coherent structures behaviour —not so the change in crop height. The modelling of coherent structures would improve the understanding of turbulence over vegetated areas, especially those devoted to agriculture. Plans to complement the findings of this paper include the use of large-eddy simulation on different land surfaces and stability regimes in order to assess the evolution of coherent structures in space and time.

Acknowledgements The authors are very grateful to the anonymous reviewers for their useful comments and constructive suggestions. This research was financed by PICT 2018-02651 and PIP-CONICET 11220130100347CO grants. Lucia Curto was supported by a fellowships granted by CONICET. The datasets generated and analysed during the current study are available from the corresponding author on reasonable request.

References

Adrian RJ (2007) Hairpin vortex organization in wall turbulence. Phys Fluids 19:041301. https://doi.org/10.1063/1.2717527

Barthlott C, Drobinski P, Fesquet C, Dubos T, Pietras C (2007) Long-term study of coherent structures in the atmospheric surface layer. Boundary-Layer Meteorol 125(1):1–24. https://doi.org/10.1007/s10546-007-9190-9

Brunet Y, Collineau S (1994) Wavelet analysis of diurnal and nocturnal turbulence above a maize crop. In: Foufoula-Georgiou E, Kumar P (eds) Wavelet analysis and its applications, vol 4. Academic Press, pp 129–150. https://doi.org/10.1016/B978-0-08-052087-2.50011-6

Chen J, Hu F (2003) Coherent structures detected in atmospheric boundary-layer turbulence using wavelet transforms at Huaihe River Basin, China. Bound-Layer Meteorol 107(2):429–444. https://doi.org/10.1023/A:1022162030155

Collineau S, Brunet Y (1993) Detection of turbulent coherent motions in a forest canopy part I: wavelet analysis. Boundary-Layer Meteorol 65(4):357–379. https://doi.org/10.1007/BF00707033
Dale M, Mah M (1998) The use of wavelets for spatial pattern analysis in ecology. J Veg Sci 9(6):805–814. https://doi.org/10.2307/3237046
Dupont S, Patton EG (2012) Influence of stability and seasonal canopy changes on micrometeorology within and above an orchard canopy: the CHATS experiment. Agric For Meteorol 157:11–29. https://doi.org/10.1016/j.agrformet.2012.01.011
Finnigan J (2000) Turbulence in plant canopies. Annu Rev Fluid Mech 32(1):519–571. https://doi.org/10.1146/annurev.fluid.32.1.519
Foken T (2017) Micrometeorology, 2nd edn. Springer, p 362
Gao W, Li B (1993) Wavelet analysis of coherent structures at the atmosphere-forest interface. J Appl Meteorol 32(11):1717–1725. https://doi.org/10.1175/1520-0450(1993)032<1717:WAOCSA>2.0.CO;2
Gao W, Shaw R, Paw UK (1989) Observation of organized structure in turbulent flow within and above a forest canopy. In: RE M (ed) Boundary Layer Studies and Applications. Springer, pp 349–377. https://doi.org/10.1007/978-94-009-0975-5_22
Horiguchi M, Hayashi T, Adachi A, Onogi S (2014) Stability dependence and diurnal change of large-scale turbulence structures in the near-neutral atmospheric boundary layer observed from a meteorological tower. Boundary-Layer Meteorol 151(2):221–237. https://doi.org/10.1007/s10546-013-9903-1
Katul G, Kuhn G, Schieldge J, Hsieh CI (1997) The ejection-sweep character of scalar fluxes in the unstable surface layer. Boundary-Layer Meteorol 83(1):1–26. https://doi.org/10.1023/A:1000293516830
Kline SJ, Reynolds WC, Schraub F, Runstadler P (1967) The structure of turbulent boundary layers. J Fluid Mech 30(4):741–773
Li D, Bou-Zeid E (2011) Coherent structures and the dissimilarity of turbulent transport of momentum and scalars in the unstable atmospheric surface layer. Boundary-Layer Meteorol 140(2):243–262. https://doi.org/10.1007/s10546-011-9613-5
Li FC, Kawaguchi Y, Hishida K (2005) Structural analysis of turbulent transport in a heated drag-reducing channel flow with surfactant additives. Int J Heat Mass Transfer 48(5):965–973. https://doi.org/10.1016/j.ijheatmasstransfer.2004.09.029
Nagano Y, Tagawa M (1988) Statistical characteristics of wall turbulence with a passive scalar. J Fluid Mech 196:157–185. https://doi.org/10.1017/S0022112088002654
Scarabino AE (2005) Características de la turbulencia atmosférica en un bosque de coníferas. PhD thesis, Universidad Nacional de La Plata
Shaw RH, Tavangar J, Ward DP (1983) Structure of the Reynolds stress in a canopy layer. J Appl Meteorol Climatol 22(11):1922–1931. https://doi.org/10.1175/1520-0450(1983)022<1922:SOTRSI>2.0.CO;2
Shaw RH, Paw UKT, Gao W (1989) Detection of temperature ramps and flow structures at a deciduous forest site. Agric For Meteorol 47(2–4):123–138. https://doi.org/10.1016/0168-1923(89)90091-9
Smedman AS, Högström U, Hunt JC, Sahlée E (2007) Heat/mass transfer in the slightly unstable atmospheric surface layer. Q J R Meteorol Soc 133(622):37–51. https://doi.org/10.1002/qj.7
Stull RB (1988) An introduction to boundary layer meteorol. Springer
Theodorsen T (1952) Mechanisms of turbulence. In: Proceedings of the 2nd Midwestern Conference on Fluid Mechanics, 1952
Thomas C, Foken T (2007) Flux contribution of coherent structures and its implications for the exchange of energy and matter in a tall spruce canopy. Boundary-Layer Meteorol 123(2):317–337. https://doi.org/10.1007/s10546-006-9144-7
Venditti JG, Hardy RJ, Church M, Best JL (2013) What is a coherent flow structure in geophysical flow? Coherent flow structures at Earth's surface, pp 1–16. https://doi.org/10.1002/9781118527221.ch1
Wallace JM (2016) Quadrant analysis in turbulence research: history and evolution. Annu Rev Fluid Mech 48:131–158. https://doi.org/10.1146/annurev-fluid-122414-034550